

Soliton gyroscopes in media with spatially growing repulsive nonlinearity

Rodislav Driben^{1,2}, Yaroslav V. Kartashov^{3,4}, Boris A. Malomed², Torsten Meier¹, and Lluís Torner³

¹*Department of Physics & CeOPP, University of Paderborn,
Warburger Str. 100, Paderborn D-33098, Germany*

²*Department of Physical Electronics, School of Electrical Engineering,
Faculty of Engineering, Tel Aviv University, Tel Aviv 69978, Israel*

³*ICFO-Institut de Ciències Fotoniques, and Universitat Politècnica de Catalunya,
Mediterranean Technology Park, E-08860 Castelldefels (Barcelona), Spain*

⁴*Institute of Spectroscopy, Russian Academy of Sciences, Troitsk, Moscow, 142190, Russia*

(Dated: August 30, 2021)

We find that the recently introduced model of self-trapping supported by a spatially growing strength of a repulsive nonlinearity gives rise to robust vortex-soliton tori, i.e., three-dimensional vortex solitons, with topological charges $S \geq 1$. The family with $S = 1$ is completely stable, while the one with $S = 2$ has alternating regions of stability and instability. The families are nearly exactly reproduced in an analytical form by the Thomas-Fermi approximation (TFA). Unstable states with $S = 2$ and 3 split into persistently rotating pairs or triangles of unitary vortices. Application of a moderate torque to the vortex torus initiates a persistent precession mode, with the torus' axle moving along a conical surface. A strong torque heavily deforms the vortex solitons, but, nonetheless, they restore themselves with the axle oriented according to the vectorial addition of angular momenta.

PACS numbers: 03.75.Lm, 05.45.Yv, 12.39.Dc, 42.65

The creation of multidimensional spatiotemporal solitons is a challenging problem of nonlinear physics, including optics and matter-wave dynamics [1]-[3]. Fundamental multidimensional solitons are prone to instabilities caused by the beam collapse [4], while vortex solitons [5] are highly vulnerable to azimuthal modulational instabilities that split them into fragments [6]. A related topic is search for various complex topological states, such as knots, “Q-balls”, “vortons”, and skyrmions, in classical-field systems [7, 8]. Those states model topological excitations in ferromagnets [9], superconductors [10], Bose-Einstein condensates (BECs) [11], and in barionic matter in the low-energy limit [12].

A few methods for the stabilization of multidimensional solitons and vortices have been put forward theoretically. These include the use of competing (cubic-quintic [13]-[15] or quadratic-cubic [16]) nonlinearities, trapping configurations [17], and, as demonstrated experimentally [18] and theoretically [19], periodic lattice potentials. The stabilization may be enhanced by “management” techniques, i.e., periodic alternation of the sign of the nonlinear term [20]. Another possibility for the stabilization is provided by the use of nonlocal nonlinearity [21].

A new approach to the creation of self-trapped fundamental and vortex solitons was recently introduced in Refs. [22, 23] and elaborated in diverse settings [24]: a repulsive (defocusing) nonlinearity, whose local strength in space of dimension D grows from the center to the periphery at any rate faster than r^D (r is the radial coordinate), supports remarkably robust families of fundamental and vortical solitons for $D = 1$ and 2. Such type of the nonlinearity modulation may be generated

by means of several techniques. In optical media, one may use inhomogeneous doping [25]. In BECs, the tunability of the magnetic Feshbach resonance (FR) [26] allows the creation of spatially inhomogeneous nonlinearity landscapes by means of properly shaped magnetic fields [1, 27]. Furthermore, optically controlled FR [28], as well as combined magneto-optical control mechanisms [29], make it possible to create a diverse set of spatial profiles of the self-repulsive nonlinearity. In particular, the required pattern of the laser-field intensity controlling the optically induced FR can be *painted* in space, as demonstrated in Ref. [30]. In terms of the above-mentioned classical field-theory models, a spatially growing component may play the role of an inhomogeneous nonlinearity coefficient for another component, coupled to the former one by a repulsive quintic interaction.

To date, self-trapping by means of the repulsive-nonlinearity scheme was studied only for to one- and two-dimensional (1D and 2D) geometries, except for the simplest case of 3D spherically symmetric solitons, which were mentioned in Ref. [23]. The objective of the present Letter is to construct stable 3D vortex tori with various topological charges S . This is a challenging goal. Thus far, limited results for stable 3D vortex tori with $S = 1$ were obtained solely in models with uniform cubic-quintic [14] and quadratic-cubic [16] focusing-defocusing nonlinearities. Only very broad vortex solitons may be stable against splitting in these systems, which makes the possibility of their experimental realization unlikely, and so far no stable 3D vortices with $S > 1$ have been found. Here we show that the family of vortex-solitons tori with $S = 1$ is completely stable, while the families with $S = 2$ and 3 feature instability segments, with the unstable tori

splitting into pairs or triangles of mutually orbiting unitary vortices. In spite of the apparent complexity of the 3D model and vortex solitons sought for, families of solutions with $S = 0$ and $S = 1, 2$ are obtained below in very accurate explicit forms by means of the variational [33, 34] and Thomas-Fermi [31] approximations (VA and TFA), respectively.

The 3D vortex-soliton tori may be viewed as matter-wave/field-theory counterparts of mechanical gyroscopes, whose most remarkable dynamical property is that application of a torque drives them into precession [32]. We find that the vortex tori in the present model behave as precessing gyroscopes under the action of a moderate torque. To the best of our knowledge, no similar effect has ever been shown for 3D vortex solitons. Furthermore, due to the robustness of the vortex-soliton tori in the setting considered here, we find that they may restore their shapes even after significant deformations caused by the application of a strong torque.

We describe the evolution of 3D matter-wave excitations by the Gross-Pitaevskii equation for the scaled wave function q :

$$i \frac{\partial q}{\partial t} = -\frac{1}{2} \nabla^2 q + \sigma(r) |q|^2 q, \quad (1)$$

where Laplacian ∇^2 acts on coordinates (x, y, z) , with $r^2 = x^2 + y^2 + z^2$, and the anti-Gaussian isotropic modulation of the local self-repulsion is chosen, $\sigma(r) = \exp(-r^2/2)$, which helps us to present the results in a compact form, although, as said above, the necessary condition for self-trapping of finite-norm modes in the 3D case is that $\sigma(r)$ must grow at $r \rightarrow \infty$ at any rate faster than r^3 . Equation (1) conserves the Hamiltonian and norm, $H = (1/2) \iiint [|\nabla q|^2 + \sigma(r) |q|^4] dx dy dz$ and $N = \iiint |q(x, y, z, t)|^2 dx dy dz$, along with the vector of the angular momentum (q^* is for the complex conjugate):

$$\mathbf{M} = -i \iiint q^* (\mathbf{r} \times \nabla) q(x, y, z) dx dy dz. \quad (2)$$

In cylindrical coordinates (ρ, z, θ) , stationary solutions with chemical potential μ and integer vorticity $S \geq 0$ are looked for as $q = \exp(-i\mu t + iS\theta) u(\rho, z)$, where the real function $u(\rho, z)$ satisfies

$$\mu u = -\frac{1}{2} \left(\frac{\partial^2 u}{\partial \rho^2} + \frac{1}{\rho} \frac{\partial u}{\partial \rho} + \frac{\partial^2 u}{\partial z^2} - \frac{S^2 u}{\rho^2} \right) + e^{(\rho^2 + z^2)/2} u^3. \quad (3)$$

The Lagrangian corresponding to Eq. (3) is $L = 2\pi \int_{-\infty}^{+\infty} dz \int_0^{\infty} \rho d\rho \mathcal{L}$, with density $\mathcal{L} = -2\mu u^2 + (\partial u / \partial \rho)^2 + (\partial u / \partial z)^2 + S^2 \rho^{-2} u^2 + e^{(\rho^2 + z^2)/2} u^4$. Families of stationary solutions are characterized by the dependence of the norm, N , on μ , while the angular momentum and norm of the solutions are related by

$$M_z = SN, M_{x,y} = 0. \quad (4)$$

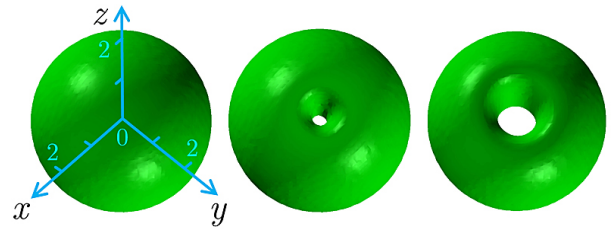


FIG. 1. (Color online) Isosurface plots for level $[u(x, y, z)]^2 = 3$ show density distributions in stable solitons with topological charges $S = 0, 1$, and 2 (left, center, and right panels, respectively), for $\mu = 16$. The respective norms are $N_0 = 246.1$, $N_1 = 225.2$, $N_2 = 191.7$.

The VA for solutions to Eq. (3) is based on the ansatz whose functional form is suggested by matching to the modulation profile in Eq. (3),

$$u_{\text{VA}}(\rho, z) = A \rho^S \exp(-(\rho^2 + z^2)/4). \quad (5)$$

Its norm is $N_S^{\text{VA}} = (2\pi)^{3/2} S! A^2$. The substitution of the ansatz into the Lagrangian leads to the variational equation, $\partial L / \partial (A^2) = 0$, to yield $A^2 = [S! / (2S)!] [\mu - (3 + 2S)/8]$. The comparison of ansatz (5) with numerically found solutions [shown below in Fig. 2(d)] indicates that the VA predicts accurate results only for $S = 0$, *viz.*,

$$N_{S=0}^{\text{VA}} = (2\pi)^{3/2} (\mu - 3/8). \quad (6)$$

For $S \geq 1$, accurate results are produced by the TFA, which was not previously applied to the description of multidimensional solitons. This approximation neglects derivatives in Eq. (3) (which is readily justified for the case of strong repulsive nonlinearity [31]), yielding

$$u_{\text{TFA}}^2 = \begin{cases} 0, & \text{at } \rho^2 < \rho_S^2 \equiv S^2 / (2\mu), \\ e^{-(\rho^2 + z^2)/2} [\mu - S^2 / (2\rho^2)], & \text{at } \rho^2 > \rho_S^2. \end{cases} \quad (7)$$

In particular, the first line in this expression corresponds to the hole at the center of a vortex state, see Fig. 2(d). The $N(\mu)$ dependence produced by Eq. (7) is

$$N_S^{\text{TFA}} = 4 (2\pi)^{3/2} \mu e^{-S^2/(4\mu)} \int_0^{\infty} dR \frac{e^{-R}}{4R + (S^2/\mu)}, \quad (8)$$

which simplifies for $S = 0$:

$$N_{S=0}^{\text{TFA}} = (2\pi)^{3/2} \mu, \quad (9)$$

cf. Eq. (6), and for $\mu \gg S^2$: $N_S^{\text{TFA}}(\mu) \approx (2\pi)^{3/2} [\mu - (S^2/4) \ln(4e\mu/S^2)]$. In the general case, the integral in Eq. (8) can be calculated numerically.

Generic examples of numerically found stable self-trapped solutions to Eq. (3), with $S = 0, 1, 2$ and $\mu = 16$, are shown in Fig. 1; families of such vortex soliton tori are represented by $N(\mu)$ curves in Fig. 2(a-c); and the

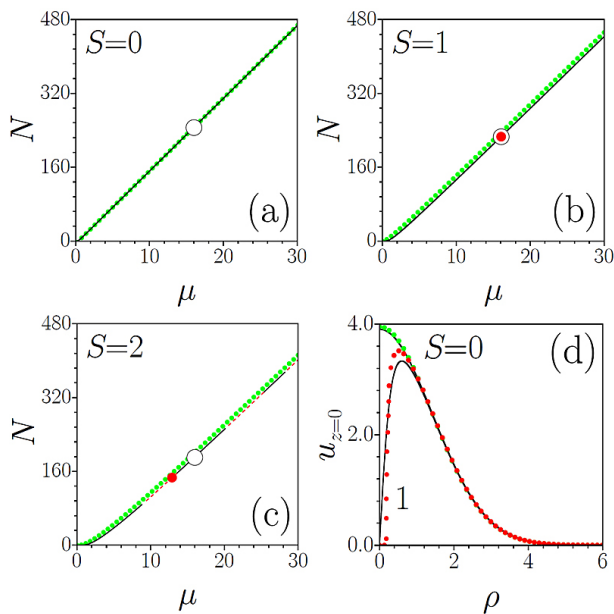


FIG. 2. (Color online) (a,b,c): Norm N versus chemical potential μ for the solitons with topological charges $S = 0, 1, 2$. Solid black and dashed red lines designate stable and unstable (for $S = 2$) branches, respectively. Green dotted lines represent the prediction of the VA in (a), and of the TFA in (b,c), see Eqs. (6) and (8), respectively. White circles designate examples of stable solutions displayed in Fig. 1. Bold red dots correspond to the vortex-soliton tori displayed in the first two rows of Fig. 3. (d) Comparison of numerically computed soliton profiles $u(\rho, z=0)$ (solid lines) with profiles predicted by the VA (green dots for $S = 0$) and TFA (red dots for $S = 1$) at $\mu = 16$.

comparison of the VA- and TFA-predicted solution profiles with their numerically found counterparts is displayed in Fig. 2(d). The stability of the solitons was checked by means of systematic simulations of the evolution of perturbed solutions. The stationary and evolutionary solutions were obtained by means of the Newton's and split-step methods, respectively, in a 3D domain of size 20^3 , covered by a mesh of 256^3 points.

As seen in Fig. 2, the VA and TFA provide very accurate predictions for the families with $S = 0$ and $S \geq 1$, respectively (for $S = 0$, the VA is slightly more accurate than the TFA). The branches with $S = 0$ and 1 were found to be completely stable, while the one with $S = 2$ (as well as its counterpart with $S = 3$, which is not shown here) features alternating regions of stability and instability. All branches satisfy the *anti-Vakhitov-Kolokolov* criterion, $dN/d\mu > 0$, which is a necessary (but, generally, not sufficient) condition for the stability of solitons supported by repulsive nonlinearities [35].

Typical examples of stable and unstable evolution of perturbed vortex-soliton tori with $S = 1, 2, 3$ are displayed in Fig. 3. In the case of unstable evolution, the phase dislocation located at the center of the vortex tori

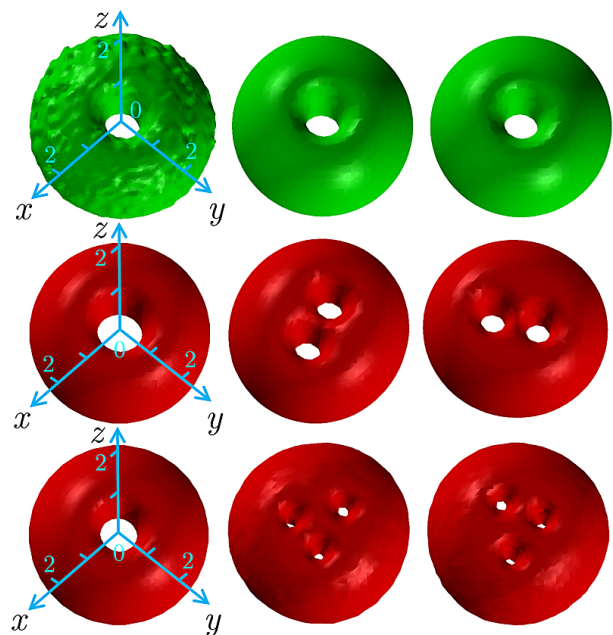


FIG. 3. (Color online) Top row: Stable evolution of a perturbed vortex-soliton torus with $S = 1$ and $\mu = 16$. Density distributions are shown at $t = 0, 450$, and 900 (from left to right). Middle row: Splitting of the unstable vortex soliton with $S = 2$, $\mu = 13$ into a steadily rotating pair of unitary vortices. Density distributions are shown at $t = 0, 230$, and 310 . Bottom row: Splitting of the unstable vortex-soliton torus with $S = 3$, $\mu = 25$ into a rotating triangle formed by unitary vortices. Density distributions are shown at $t = 0, 165$ and 180 . In the top and middle rows, and in the bottom one isosurfaces correspond to $|q(x, y, z)|^2 = 2.5$ and $|q(x, y, z)|^2 = 3$, respectively.

splits into a pair (for $S = 2$) or a triangle (for $S = 3$) of charge-1 dislocations, which rotate around the z -axis. The total moment (2) is conserved in the course of the evolution. This instability scenario is in contrast to those for vortex solitons in other models with local nonlinearities, where vortex solitons split into sets of separating vorticityless fragments [6, 14, 16, 36]. The splitting of 2D higher-order solitary vortices into separating unitary ones in a nonlocal liquid-crystal model was demonstrated in Ref. [36] (while here the split unitary vortices remain bound).

The above results suggest that 3D vortex-soliton tori may feature dynamics similar to that of mechanical gyroscopes. A salient property of gyroscopes is that the application of a torque perpendicular to the original angular momentum causes their precessing motion [32]. The vortex solitons considered here share this property. To elucidate it, a torque, with the angular momentum directed along axis y , was applied by multiplying the wave function of a stable vortex soliton, whose axle is directed along z , by

$$T = \exp(i\alpha z \tanh(x/x_0)). \quad (10)$$

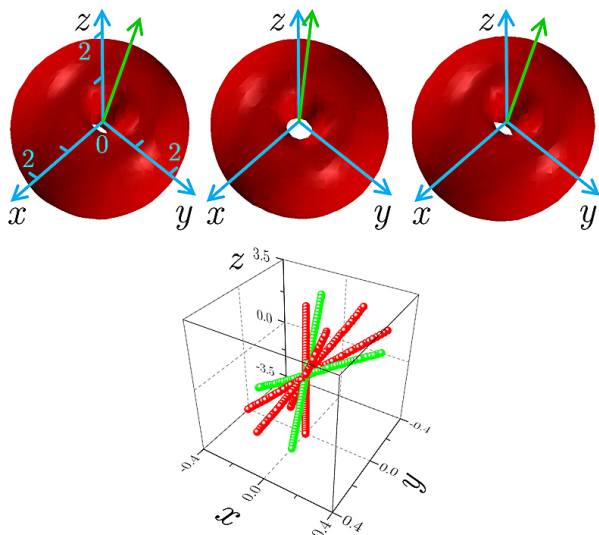


FIG. 4. (Color online) Precession of a vortex soliton (with $S = 1$) initiated by a relatively weak torque (10), with $\alpha = 4$ and $x_0 = 5$. Top row: Isosurface plots at $t = 90, 90.8$, and 91.5 (from left to right), time $\Delta t = 1.5$ between the first and last panels being the precession period. Green arrows indicate respective orientations of the axle of the torus. Bottom row: Positions of the axle at different moments of time, within one precession period. The positions shown in green correspond to the configurations displayed in the top row.

When the torque is relatively small, it induces a periodic precession of the axle of the vortex-soliton torus along a slightly deformed conical surface, as shown in Fig. 4. The central axis of the cone coincides with the direction of the total angular momentum, which is the vectorial sum of the original momentum (4) and the torque momentum corresponding to factor (10). The latter component can be found in an analytical form for the case when the shape (10) is smooth, with large x_0 , and the form of the vortex-soliton torus is taken as per Eq. (7): $M_y = (\alpha/2x_0) [N_S - (2\pi)^{3/2} (\mu - S^2/4)]$. Note that this expression vanishes for fundamental solitons, with $S = 0$, as follows from Eq. (9).

The precession of 3D vortex solitons, which, to the best of our knowledge, was never shown in previous works, is analogous to the precession motion of mechanical gyroscopes. An notable difference in the dynamics of the vortex-soliton gyroscopes from their mechanical counterparts is the reaction to a strong torque. A typical example is shown in Fig. 5, where application of a strong torque apparently deforms the vortex torus beyond recognition. Nevertheless, a close inspection of its phase profile at $z = 0$, displayed in the left bottom panel, and a related density profile (not shown here) indicates that the deformed object keeps the inner vorticity, along with the corresponding inner hole, whose environs are strongly deformed by the perturbation. The simulations reveal that, in the course of the subsequent evolution, the shape of

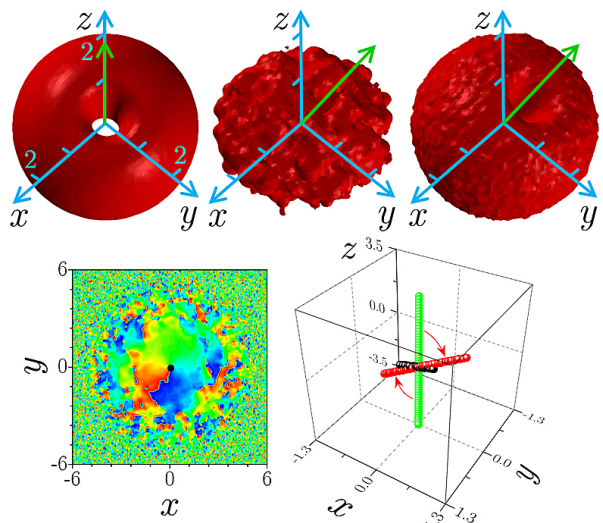


FIG. 5. (Color online) Top row: Isosurface plots, drawn at $|q(x, y, z)|^2 = 2.5$, show the violent deformation of the vortex-soliton torus, with $S = 1$ and $\mu = 10$, by a torque (10) with $\alpha = 10$ and $x_0 = 3$, followed by its gradual recovery. The three plots pertain to $t = 0, 3$, and 60 , from left to right, with the green arrows indicating the respective orientations of the axle of the torus (at $t = 3$, this is actually the local orientation at the torus center, the axle being strongly deformed in this configuration). Bottom row, left: The phase distribution in the cross section $z = 0$ at $t = 3$ (left), with the bold dot showing the position of the axle. Right: arrows show the effective rotation of the axle from its initial direction (green) at $t = 0$ to the final one at $t = 60$ (red). The black segment shows a short central fragment of the curved axle of the strongly deformed torus at $t = 3$.

the vortex-soliton torus is gradually restored, with the straight axle aligned parallel to the total angular momentum, which is the sum of the original momentum and that added by the impulse. The resulting rotation of the axle from the initial to the final position is highlighted by arrows in the right bottom panel of Fig. 5. Such evolution is a direct indication of a surprisingly high robustness of the vortex soliton tori – at least, for $S = 1$.

In conclusion, we have found that a self-repulsive cubic nonlinearity, whose strength grows from the center to periphery in the 3D space faster than r^3 (which may be implemented in BEC and in field theories with diverse physical realizations), gives rise to robust vortex-soliton tori – at least, those with topological charges $S = 1$ and 2 . Unstable solutions with $S \geq 2$ split into rotating states with nested single-charged vortices. We have found that application of a moderately strong torque sets the vortex solitons into gyroscopic precession, with the axle moving along a conical surface. Strong torques heavily deform the initial states, but, even under such perturbations, the vortex-soliton tori gradually restore themselves, with the axle directed along the total angular momentum. To the best of our knowledge, such gyroscopic dynamics of

vortex solitons have not been encountered earlier in any comparable model.

B.A.M. appreciates hospitality of ICFO. The work of R.D. and B.A.M. was supported, in a part, by the Binational (US-Israel) Science Foundation through grant No. 2010239, and by the German-Israel Foundation through grant No. I-1024-2.7/2009. R.D. and T.M. acknowledge support provided by the Deutsche Forschungsgemeinschaft (DFG) via the Research Training Group (GRK 1464).

-
- [1] B. A. Malomed, D. Mihalache, F. Wise, and L. Torner, *J. Optics B: Quant. Semicl. Opt.* **7**, R53 (2005).
- [2] D. Mihalache, *J. Optoelect. Adv. Mat.* **12**, 12 (2010).
- [3] Y. V. Kartashov, B. A. Malomed, and L. Torner, *Rev. Mod. Phys.* **83**, 247 (2011).
- [4] L. Bergé, *Phys. Rep.* **303**, 259 (1998); E. A. Kuznetsov and F. Dias, *ibid.* **507**, (2011).
- [5] A. S. Desyatnikov, L. Torner, and Y. S. Kivshar, *Progr. Opt.* **47**, 1 (2005).
- [6] W. J. Firth and D. V. Skryabin, *Phys. Rev. Lett.* **79**, 2450 (1997); L. Torner and D. Petrov, *Electron. Lett.* **33**, 608 (1997); Yu. S. Kivshar and D. E. Pelinovsky, *Phys. Rep.* **331**, 117 (2000).
- [7] L. Faddeev and A. J. Niemi, *Nature* **387**, 58 (1997); H. Aratyn, L. A. Ferreira, and A. H. Zimerman, *Phys. Rev. Lett.* **83**, 1723 (1999); D. J. Gross and N. A. Nekrasov, *J. High Energy Phys.* **3**, 044 (2001); B. Kleihaus, J. Kunz, and Y. Shnir, *Phys. Rev. D* **68**, 101701 (2003); J. Kunz, U. Neemann, and Y. Shnir, *Phys. Lett. B* **640**, 57 (2006).
- [8] E. Radu and M. S. Volkov, *Phys. Rep.* **468**, 101 (2008).
- [9] N. R. Cooper, *Phys. Rev. Lett.* **82**, 1554 (1999).
- [10] E. Babaev, *Phys. Rev. Lett.* **88**, 177002 (2002).
- [11] J. Ruostekoski and J. R. Anglin, *Phys. Rev. Lett.* **86**, 3934 (2001); R. A. Battye, N. R. Cooper, and P. M. Sutcliffe, *ibid.* **88**, 080401 (2002); J. Ruostekoski, *Phys. Rev. A* **70**, 041601(2004); K. Kasamatsu, M. Tsubota, and M. Ueda, *Int. J. Mod. Phys. B* **19**, 1835 (2005); Y. M. Cho, H. Khim, and P. M. Zhang, *Phys. Rev. A* **72**, 063603 (2005); M. Nitta, K. Kasamatsu, M. Tsubota, and H. Takeuchi, *ibid.* **A 85**, 053639 (2012); T. Kawakami, T. Mizushima, M. Nitta, K. Machida, *Phys. Rev. Lett.* **109**, 015301 (2012).
- [12] R. Alkofer, H. Reinhardt, and H. Weigel, *Phys. Rep.* **265**, 139 (1996); M. Bender, P. H. Heenen, and P. G. Reinhard, *Rev. Mod. Phys.* **75**, 121 (2003).
- [13] M. Quiroga-Teixeiro and H. Michinel, *J. Opt. Soc. Am. B* **14**, 2004 (1997); M. L. Quiroga-Teixeiro, A. Berntson, and H. Michinel, *ibid.* **16**, 1697 (1999); R. L. Pego and H. A. Warchall, *J. Nonlinear Sci.* **12**, 347 (2002); H. Michinel, J. Campo-Taboas, R. Garcia-Fernandez, J. R. Salgueiro, M. L. Quiroga-Teixeiro, *Phys. Rev. E* **65**, 066604 (2002); T. A. Davydova and A. I. Yakimenko, *J. Opt. A: Pure Appl. Opt.* **6**, S197 (2004);
- [14] D. Mihalache *et al.*, *Phys. Rev. Lett.* **88**, 073902 (2002); D. Mihalache *et al.*, *J. Opt. B* **6**, S333 (2004).
- [15] K. Dimitrevski *et al.*, *Phys. Lett.* **248**, 369 (1998).
- [16] D. Mihalache *et al.*, *Phys. Rev. E* **66**, 016613 (2002).
- [17] F. Dalfovo and S. Stringari, *Phys. Rev. A* **53**, 2477 (1996); R. J. Dodd, *J. Res. Natl. Inst. Stand. Technol.* **101**, 545 (1996); T. J. Alexander and L. Bergé, *Phys. Rev. E* **65**, 026611 (2002); D. Mihalache, D. Mazilu, B. A. Malomed, and F. Lederer, *Phys. Rev. A* **73**, 043615 (2006).
- [18] D. Neshev *et al.*, *Phys. Rev. Lett.* **92**, 123903 (2004); J. W. Fleischer *et al.*, *ibid.* **92**, 123904 (2004).
- [19] N. K. Efremidis, S. Sears, D. N. Christodoulides, J. W. Fleischer, and M. Segev, *Phys. Rev. E* **66**, 046602 (2002); B. B. Baizakov, B. A. Malomed, and M. Salerno, *Europhys. Lett.* **63**, 642 (2003); J. Yang and Z. H. Musslimani, *Opt. Lett.* **28**, 2094 (2003); D. Mihalache *et al.*, *Phys. Rev. E* **70**, 055603(R) (2004); D. Mihalache *et al.*, *Phys. Rev. Lett.* **95**, 023902 (2005); R. Driben, B. A. Malomed, A. Gubeskys, and J. Zyss, *Phys. Rev. E* **76**, 066604 (2007); R. Driben and B. A. Malomed, *Eur. Phys. J. D* **50**, 317 (2008).
- [20] G. D. Montesinos, V. M. Pérez-García, H. Michinel, and J. R. Salgueiro, *Phys. Rev. E* **71**, 036624 (2005); B. A. Malomed, *Soliton Management in Periodic Systems* (Springer: New York, 2006).
- [21] A. W. Snyder and D. J. Mitchell, *Science* **276**, 1538 (1997); G. Assanto and M. Peccianti, *IEEE J. Quant. Electr.* **39**, 13 (2003); D. Mihalache, *et al.*, *Phys. Rev. E* **73**, 025601 (2006); V. M. Lashkin, A. I. Yakimenko, and O. O. Prihodko, *Phys. Lett. A* **366**, 422 (2007); G. Assanto, T. R. Marchant, and N. F. Smyth, *Phys Rev A* **78**, 063808 (2008); W.-P. Zhong and M. Belić, *ibid.* **79**, 023804 (2009); F. Maucher *et al.*, *Phys. Rev. Lett.* **106**, 170401 (2011).
- [22] O. V. Borovkova, Y. V. Kartashov, B. A. Malomed, and L. Torner, *Opt. Lett.* **36**, 3088 (2011).
- [23] O. V. Borovkova, Y. V. Kartashov, L. Torner, and B. A. Malomed, *Phys. Rev. E* **84**, 035602 (R) (2011).
- [24] Y. V. Kartashov, V. A. Vysloukh, L. Torner, and B. A. Malomed, *Opt. Lett.* **36**, 4587 (2011); V. E. Lobanov, O. V. Borovkova, Y. V. Kartashov, B. A. Malomed, and L. Torner, *ibid.* **37**, 1799 (2012); Q. Tian, L. Wu, Y. Zhang, and J.-F. Zhang, *Phys. Rev. E* **85**, 056603 (2012); Y. Wu, Q. Xie, H. Zhong, L. Wen, and W. Hai, *ibid.* **A 87**, 055801 (2013); W. B. Cardoso, J. Zeng, A. T. Avelar, D. Bazeia, and B. A. Malomed, *Phys. Rev. E* **88**, 025201 (2013).
- [25] J. Hukriede, D. Runde, and D. Kip, *J. Phys. D* **36**, R1 (2003).
- [26] G. Roati *et al.*, *Phys. Rev. Lett.* **99**, 010403 (2007); S. E. Pollack *et al.*, *ibid.* **102**, 090402 (2009).
- [27] F. K. Abdullaev, A. Gammal, and L. Tomio, *J. Phys. B: At. Mol. Opt. Phys.* **37**, 635 (2004); H. Sakaguchi and B. A. Malomed, *Phys. Rev. E* **72**, 046610 (2005); F. K. Abdullaev and J. Garnier, *Phys. Rev. A* **72**, 061605(R) (2005).
- [28] P. O. Fedichev, Yu. Kagan, G. V. Shlyapnikov, and J. T. M. Walraven, *Phys. Rev. Lett.* **77**, 2913 (1996); M. Yan, B. J. DeSalvo, B. Ramachandran, H. Pu, and T. C. Killian, *Phys. Rev. Lett.* **110**, 123201 (2013).
- [29] D. M. Bauer, M. Lettner, C. Vo, G. Rempe and S. Dürr, *Nature Phys.* **5**, 339 (2009).
- [30] K. Henderson, C. Ryu, C. MacCormick, and M. G. Boshier, *New J. Phys.* **11**, 043030 (2009).
- [31] T. L. Ho and V. B. Shenoy, *Phys. Rev. Lett.* **77**, 3276 (1996); H. Pu, and N. P. Bigelow, *ibid.* **80**, 1130 (1998); M. Trippenbach, K. Goral, K. Rzazewski, B. Malomed, and Y. B. Band, *J. Phys. B: At. Mol. Opt. Phys.* **33**,

- 4017 (2000).
- [32] L. D. Landau and E. M. Lifshitz, *Mechanics* (Moscow: Nauka publishers, 1988).
- [33] M. Desaix, D. Anderson, and M. Lisak, *J. Opt. Soc. B* **8**, 2082 (1991).
- [34] V. M. Pérez-García, H. Michinel, J. I. Cirac, M. Lewenstein, and P. Zoller, *Phys. Rev. A* **56**, 1424 (1997); J. O. Andersen, *Rev. Mod. Phys.* **76**, 599 (2004).
- [35] H. Sakaguchi and B. A. Malomed, *Phys. Rev. A* **81**, 013624 (2010).
- [36] A. A. Minzoni, L. W. Sciberras, N. F. Smyth, and A. L. Worthy, in: G. Assanto, editor, *Spatial Optical Solitons in Nematic Liquid Crystals*, chapter 15 (John Wiley and Sons: New York, 2012).